Atmospheric Environment 338 (2024) 120839

Contents lists available at ScienceDirect

Atmospheric Environment

journal homepage: www.elsevier.com/locate/atmosenv

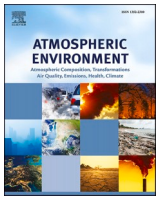

In silico modelling of radiative efficiencies of anthropogenic greenhouse gases

Daniela Alvarado-Jiménez [a,b], Nicola Tasinato [a,*]

[a] *Scuola Normale Superiore, I-56126, Pisa, Italy*
[b] *IUSS Scuola Universitaria Superiore, I-27100, Pavia, Italy*

HIGHLIGHTS

- Radiative efficiencies (REs) climate metrics to understand greenhouse gas impact.
- Cost-effective computational methodology for predicting greenhouse-gas REs.
- Full account for anharmonic contributions, without any empirical adjustment.
- Accuracy on REs of 5%, on par with the most refined experimental determinations.
- In silico prediction of policy relevant data and for screening replacement compounds.

GRAPHICAL ABSTRACT

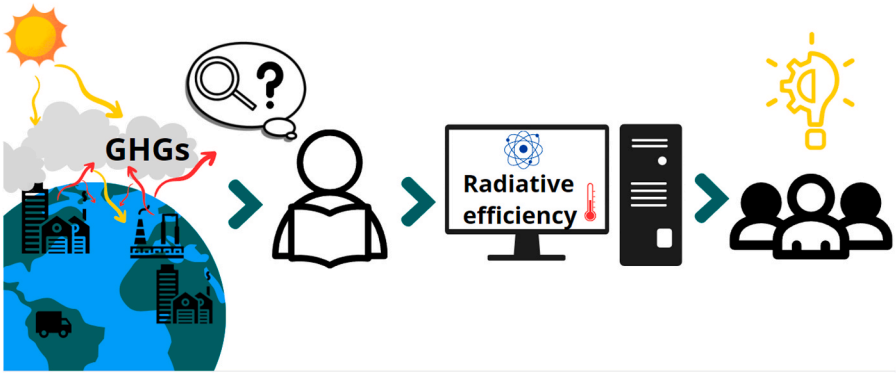

ARTICLE INFO

Keywords:
Radiative forcing
Halocarbons
Quantum chemistry
Infrared spectroscopy
Climate metrics

ABSTRACT

Radiative efficiency (RE) is a climate metric adopted in international reports on climate change to quantify the greenhouse capacity of gases, and hence to guide decision-making processes and drive transitions in the production and utilization of chemicals in different application fields. Key quantities for the determination of the RE of a gas are the atmospheric irradiance profile and the infrared (IR) absorption cross section spectrum. The latter is usually measured experimentally, even though acquiring high-quality IR spectra can pose severe challenges, sometimes limiting the accuracy or the accessible spectral range. While computational quantum chemistry methods have emerged as valuable tools to simulate IR absorption properties, their application to REs estimation is still limited to the use of the double-harmonic approximation, which presents fundamental limitations. In this work, a cost-effective quantum chemical (QC) workflow including non-empirical anharmonic contributions to spectral properties and an automatic identification of conformer distribution is presented for the accurate evaluation of REs using a range of atmospheric irradiance profiles. Different levels of theory are considered, according to the current state-of-the-art, and the accuracy of the QC RE tool is demonstrated with reference to a number of representative halocarbons widely used in refrigeration, manufacturing, and pharmaceutical fields.

* Corresponding author.
E-mail address: nicola.tasinato@sns.it (N. Tasinato).

https://doi.org/10.1016/j.atmosenv.2024.120839
Received 13 May 2024; Received in revised form 22 September 2024; Accepted 23 September 2024
Available online 25 September 2024

The results show that REs can be computed with an average accuracy of 5% using double-hybrid functionals, which overshoot the widely used B3LYP method. Finally, the QC methodology is applied to determine the REs of selected halocarbons for which data is limited, or to address some contradictory results appeared in the literature for some species. The outcomes of this work demonstrate that QC anharmonic IR cross section spectra can be used to estimate REs with an accuracy on par with that of experimental measurements, hence applicable to challenging cases for providing data for policymakers as well for screening purposes when seeking new replacement compounds.

1. Introduction

Radiative forcing (RF) is a fundamental notion in climate science which quantifies the strength of the different anthropogenic and natural drivers of climate change, thus being instrumental in understanding the perturbations imposed on the Earth's climate system. As defined by the Intergovernmental Panel on Climate Change (IPCC), RF represents the externally induced energy imbalance within the climate system, capable of causing climate parameter changes and ultimately leading to a new equilibrium state (Forster et al., 2021). The global mean RF is indeed strictly connected to the change in the mean surface temperature. In addition, together with atmospheric lifetimes, radiative efficiencies (RE), namely the RF per molecule, are input parameters for evaluating the global warming potential (GWP) (González et al., 2016; Sharma et al., 2019; Wallington et al., 2015) that measures, on a CO_2-equivalent scale, the greenhouse capacity of non-CO_2 gases. GWPs, which have been adopted in international agreement since the Kyoto protocol in 1997, are collected and continuously updated in IPCC (The Intergovernmental Panel on Climate Change) and World Meteorological Organization (WMO) reports (World Meteorological Organization (WMO)). The concept of RF has evolved over time together with our knowledge of climate perturbing agents, and currently different flavours of the RE metrics exist (Andrews et al., 2021). The so-called instantaneous RE (IRE) measures the RF for a unit gas pulse without considering adjustments due to fast responses to climate change drivers. The effective radiative efficiency (ERE) measures the top-of-atmosphere energy budget changes following adjustments to the vertical temperature profile, clouds, and land-surface temperatures (Anthropogenic and Natural Radiative Forcing, 2014; Ramaswamy et al., 2019). EREs are more representative than IRE of temperature changes, however, they are more uncertain as they rely on climate model estimates of cloud response (Sherwood et al., 2015).

Increasing atmospheric concentrations of CO_2, CH_4 and N_2O are the widely recognized major drivers of radiative forcing of climate change, nonetheless alongside this, halocarbons and related compounds make a significant contribution, their RF being estimated to be 0.41 W m^{-2}, about 20% that of CO_2 (Forster et al., 2023; Hodnebrog et al., 2020). Among halocarbons, chlorofluorocarbons (CFCs) gained widespread usage in various daily-life sectors since the 1950s, but their capacity to catalytically destroy the stratospheric ozone layer led to international measures to control their use (Reimann et al., 2018). The Montreal Protocol (1987) aimed to regulate and eventually ban these substances (United Nations Environment Programme). As alternatives to CFCs, hydrochlorofluorocarbons (HCFCs), hydrofluorocarbons (HFCs) and perfluorocarbons (PFCs) were introduced due to their reduced (HCFCs) or zero (HFCs, PFCs) ozone depletion potential (Midgley, 1997). However, they were later recognized as powerful greenhouse gases (GHG) (World Meteorological Organization (WMO), 2014) and, in 2006, the Kigali Amendment to the Kyoto Protocol called for the phasedown of these species (Chen et al., 2023). This is because, halogenated, and especially fluorinated compounds, which are widely used as refrigerants, blowing agents, cleaning solvents, anesthetics, and reactants for the synthesis of fine chemicals (Kim et al., 2011), strongly absorb the infrared (IR) radiation within the 800–1200 cm^{-1} atmospheric window, in which absorptions by H_2O, CO_2 and O_3 are minimum. This window furthermore overlaps with the peak in the terrestrial thermal spectrum (500–1500 cm^{-1}), making it particularly important in the radiative balance of the atmosphere (Pinnock et al., 1995).

The fundamental information necessary to determine the RE of a molecule is the IR absorption cross section spectrum which, therefore, needs to be experimentally measured with high accuracy, thus implying among others, a precise control of the experimental conditions (Sharpe et al., 2004; Tasinato et al., 2010a; Wallington et al., 2009). While well trusted data with accuracy of 5% or better are of primary importance, obtaining high-quality IR spectra experimentally presents many challenges, including impurities, temperature control, pressure measurements, path lengths limitations, and potential equipment errors (Blowers and Hollingshead, 2009; Coheur et al., 2003). Those requirements are intrinsically very difficult to meet for species with low vapor pressures (i.e. less-volatile substances).

Computational quantum chemistry, on the other hand, has emerged as a tool to simulate molecular properties, including longwave spectral features. The predictive and interpretative ability of computational quantum chemistry is demonstrated by state-of-the-art approaches to spectroscopy (Puzzarini et al., 2019) that, provided the main physical factors are properly accounted for (Barone et al., 2023; Ceselin et al., 2022; Tasinato et al., 2017), can yield results comparable to the most accurate experimental techniques (Li et al., 2018; Tasinato et al., 2012). While quantum chemical (QC) methods have already been applied to the estimation of REs (Blowers et al., 2008a; Blowers and Hollingshead, 2009; Bravo et al., 2010, 2011; Holtomo et al., 2022; Papanastasiou et al., 2018; Papasavva et al., 1995; van Hoomissen et al., 2023), they have been limited to the double-harmonic approximation which is known to present a number of limitations and it cannot deliver an accuracy comparable to experimental measurements. As a matter of fact, it yields predicted vibrational frequencies that can deviate significantly from experimental observations, and it completely neglects overtone and combination transitions. To mitigate the overestimation of transition frequencies, it is common to apply empirical scaling factors (Alecu et al., 2010), usually determined through a least-squares fitting procedure involving a set of experimental vibrational frequencies. This operation, however, cannot recover for the missing transitions nor introduce anharmonic contributions into absorption cross sections (i.e. transitions intensities). In this respect, Burkholder et al. have pointed out that HFC IR transitions strengths are overestimates from 5% to 20% by the double-harmonic approximation, depending on the molecule considered (Burkholder et al., 2020). The limitations affecting the double-harmonic approximation can, de facto, raise questions about the accuracy of the computed REs, especially in comparison to those obtained experimentally. In fact, about 45 halocarbons were discarded from the 2013 to the 2020 compilations of global warming potentials because of the untrustable accuracy of the REs computationally obtained within the harmonic approximation (Hodnebrog et al., 2020). A full QC account of anharmonicity has the advantage of providing a more accurate representation of both transition frequencies and intensities for singly excited vibrations, as well as for transitions involving the simultaneous excitation of two or more vibrational quanta (Carnimeo et al., 2013; Puzzarini et al., 2019; Tasinato et al., 2012).

Within this background, the present work aims at developing and applying a physically sounded and cost-effective QC method to determine the REs of greenhouse gases with an accuracy comparable to experimentally based measurements. Additionally, while the necessity

to account for different conformers in evaluating the longwave properties of greenhouse gases, particularly halogenated ethers and esters, has been questioned, attention must be paid in generalizing this conclusion as it is rather case-specific. Therefore, the proposed approach also implements an automatic search of meaningful and energetically significant conformers, thus leading to the computational workflow schematized in Fig. 1, which, as described in the following, presents only one empirical parameter. The computational workflow is also equipped with different RF of the global annual mean atmosphere (GAM) and accounts for both lifetime correction and stratospheric temperature adjustment. The accuracy and reliability of the QC procedure is demonstrated by considering a range of representative halocarbons including CFCs, HCFCs, HFCs, hydro-fluoro- and hydro-chloro-fluoro-ethers (HFE and HCFE, respectively) and halons. Finally, application to selected species of atmospheric and industrial relevance for which literature data is contradictory or limited, is presented with the aim of showing the robustness of the procedure and its use for providing reliable data for policy regulations and for screening replacement compounds.

2. Methods

The quantum chemical evaluation of the longwave radiative properties of the target molecular species was carried out by using different methods rooted into density functional theory (DFT) to assess their accuracy in determining radiative efficiencies. The double-hybrid density functionals (DFs) B2PLYP (Grimme, 2006), DSDPBEP86 (Santra et al., 2019), and rev-DSDPBEP86 (Santra et al., 2019) were used in conjunction with the jun-cc-pV(T+*d*)Z (Papajak et al., 2011) basis set because of their accuracy in predicting structural and spectroscopic properties (Barone et al., 2020; Boussessi et al., 2020). In addition, the meta-hybrid PW6B95 DF (Zhao and Truhlar, 2005) was employed in conjunction with the jul-cc-pV(*n*+d)Z (Papajak et al., 2011) basis sets, with n = D and T. The popular B3LYP (Becke, 1993) functional was also considered because of its widespread use and for being one of the methods of choice in previous studies on theoretical RE evaluation. For the Br atom, the aug-cc-pV*n*Z-PP (n = D, T) basis set (Peterson et al., 2003, 2006) including pseudo-potentials was employed as downloaded from the Basis Set Exchange library (Pritchard et al., 2019; https://www.basissetexchange.org/. Last access on 28 August 2024). All DFs were augmented by the Grimme's DFT-D3 scheme for dispersion energies (Grimme et al., 2010). Equilibrium geometries were optimized at first and then harmonic and anharmonic transition frequencies and intensities were computed on the resulting geometry. Second-order vibrational perturbation theory (VPT2) (Papoušek and Aliev, 1982) was used for the purpose, because of the trade-off between accuracy and computational cost. Accidental near degeneracies due to anharmonic resonances between vibrational energies, that can plague the perturbation expressions, were solved by adopting the so-called generalized VPT2 (GVPT2) framework (Barone, 2004; Bloino et al., 2012). All calculations and GVPT2 treatments were performed using the Gaussian 16 suite of programs (Frisch et al., 2016).

For molecules characterized by different torsional degrees of freedom, an automatic sampling of the conformational landscape was performed by using the CREST computer code (Pracht et al., 2020) to identify the low-energy conformers. Basically, the software samples the

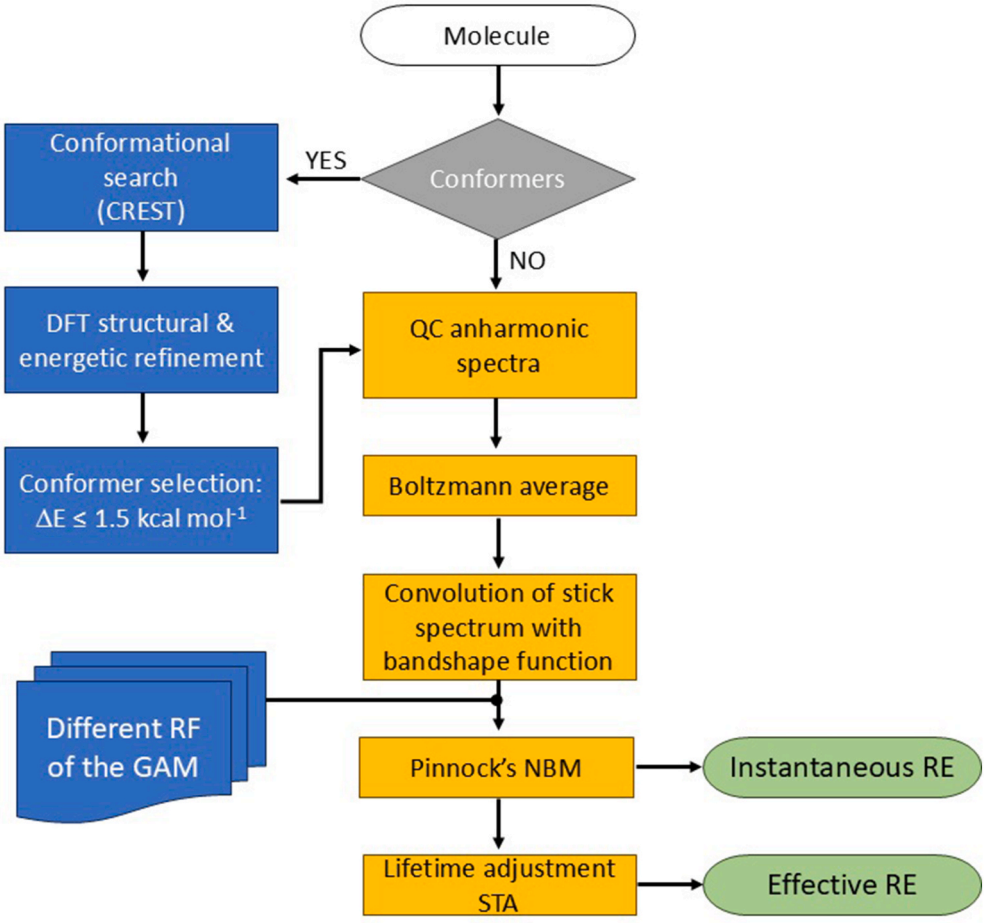

Fig. 1. Computational workflow for the quantum chemical evaluation of REs including non-empirical treatment of anharmonicity for both IR transition frequencies and intensities and automatic inclusion of conformer distribution.

chemical space making use of a meta-dynamics search algorithm (Grimme, 2019) relying on the GFN-xTB semiempirical tight-binding method (Grimme et al., 2017) which allows efficient computations for systems containing up to hundreds of atoms. For the conformational search, the molecular structure was preliminary optimized at the GFN2-xTB level, and the resulting geometry was then fed into the iterative meta-dynamics genetic structure crossing algorithm (Hibbert, 1993; Leardi, 2001; Vainio and Johnson, 2007), which was used with standard settings. In this way, the low-energy conformational ensemble within a 6 kcal mol^{-1} from the global minimum was obtained. As pointed out in the original work (Pracht et al., 2020), the choice of a 6 kcal mol^{-1} energy windows is justified because of the different morphology in the conformational landscape at the semi-empirical and QC levels. The identified conformer candidates were then subjected to post-optimization and frequency computation at the DSDPBEP86-D3/-jun-cc-pV(T+*d*)Z level to obtain accurate structures (with some GFN2-xTB candidates collapsing to the same QC conformer) and free energies. Finally, only the conformers lying within an energy window of 1.5 kcal mol^{-1} were retained for subsequent anharmonic computations (see Fig. 1).

REs were calculated on the basis of the Pinnock's narrow band model (NBM) (Pinnock et al., 1995) according to Equation (1):

$$RE = \sum_{i=1}^{n} \left[\int_{\nu_{1,i}}^{\nu_{2,i}} \sigma_i(\nu) d\nu \right] F_{\sigma}^{i} \tag{1}$$

where F_{σ}^{i} is the radiative forcing per unit cross section of the GAM in the spectral interval *i*, and σ_i is the integrated cross section over the same range. In this study, rather than relying on experimental integrated absorption cross sections, we employed anharmonic intensities obtained through computational methods. It follows that, once defined the RF of the GAM, the molecule's IRE can be evaluated from its IR cross section spectrum, which was obtained by convoluting the computed stick spectra with either Gaussian (Equation (2)) or Lorentzian normalized functions with half-width at half-maximum (HWHM) of 10, 20 and 30 cm^{-1}:

$$f(x) = \frac{1}{\sqrt{\pi}} e^{-x^2} \tag{2}$$

$$f(x) = \frac{1}{\pi} \frac{HWHM/\alpha_D}{\left(HWHM/\alpha_D\right)^2 + x^2} \tag{3}$$

where $x = \nu - \nu_0/\alpha_D$ being ν the wavenumber, ν_0 the transition frequency and α_D the Napierian HWHM (Tasinato et al., 2010b). Some tests were also performed using a narrower HWHM of 5 cm^{-1} obtaining essentially the same results as for the 10 cm^{-1} half-width. Since the fine ro-vibrational structure is neglected, the use of broadening functions effectively simulated the spectral band-shape used for the calculation of the integrated anharmonic absorption cross section over the series of integration intervals as required by the NBM in the range 0–3000 cm^{-1}. The calculation of REs was conducted using a home-made software. The program processes the output files obtained from QC calculations for the different conformers, extracts relevant information, including Boltzmann averages according to the relative Gibbs free energies.

With reference to Equation (1), we employed different models of GAM (F_{σ}^{i}), as obtained by Pinnock et al. (Pinnock et al., 1995), Hodnebrog et al. (Hodnebrog et al., 2013) and Shine and Myhre (2020). Some of the updates introduced by Hodnebrog et al. (Hodnebrog et al., 2013) included recalculating the Pinnock's curve using area-weighted results derived from one tropical and two extratropical profiles, in contrast to a single global mean profile. The GAM worked out by Shine and Myhre (2020) and used in the 2020 update of EREs (and GWP) (Hodnebrog et al., 2020) included stratospheric temperature adjustment (STA) and an improved representation of water vapor and clouds. Including those different models was crucial to ensure the coherence of our findings. The instantaneous radiative forcing developed by Pinnock et al. (Pinnock et al., 1995) assumes an atmospheric well-mixed distribution of gases across altitude and latitude. However, it has been shown that when such conditions are not met, a correction term for the gas lifetime (τ) needs to be introduced, which accounts for variables like emission distribution and varying vertical profiles (Hodnebrog et al., 2013). Equations (4) and (5) present the gas lifetime corrections, depending on whether the dominant removal process is OH degradation (for gases with lifetimes ranging from $10^{-4} < \tau < 10^{4}$ years) or photolysis ($10 < \tau < 10000$ years), respectively (Hodnebrog et al., 2013):

$$f(\tau) = \frac{2.962\tau^{0.9312}}{1 + 2.994\tau^{0.9302}} \tag{4}$$

$$f(\tau) = 1 - 0.1826\tau^{-0.3339} \tag{5}$$

In the present work, the lifetime correction was applied to ensure the reliability of our results and validate the *in silico* methodology against the REs taken from Hodnebrog et al., 2013, 2020 which have been preferred over those provided by van Hoomissen et al. (van Hoomissen et al., 2023) to avoid mixing theoretical estimates and experimental measurements in reference data used for validation purposes. Indeed, the latter set makes use of the compilations of refs. (Hodnebrog et al., 2020) and (Hodnebrog et al., 2013) and uses theoretical values, obtained within the harmonic approximation, to correct experimental REs and account for the low frequency IR absorptions.

The importance of including STA in RE calculations has been pointed out by Hodnebrog et al. (2013) and Shine and Myhre (2020). Halocarbons contribute to warm the lower stratosphere because of their strong absorptions within the atmospheric window (extra absorption of upwelling radiation exceeds the extra radiation emitted). As a result, higher stratospheric temperatures cause an increase in the downward emission of radiation into the troposphere. This adjustment leads to a stratosphere-adjusted forcing that exceeds the instantaneous forcing. To account for this effect, Hodnebrog et al. (2013) applied a generic 10% increase to all REs. Later, Shine and Myhre developed an updated GAM that inherently embraced stratospheric adjustment and highlighted the importance of including a wavenumber dependent correction (Shine and Myhre, 2020). Indeed, an increase in the concentration of a GHG that absorbs in opaque spectral regions (<750 cm^{-1}) and near the ozone absorption (around 1000 cm^{-1}) causes a cooling in the stratosphere, and consequently a RF up to 40% lower than the IRF. In contrast, the increasing GHG levels result in a positive contribution of about 10% compared to the IRF within the atmospheric window (excluding the ozone bands region). As for lifetime corrections, to ensure the consistency of our approach and to validate it, a 10% STA was applied to REs when using reference values taken from Hodnebrog et al. (2013), whereas no adjustment was used when comparing to Hodnebrog et al. (2020) being this already accounted for in the GAM (Hodnebrog et al., 2013; Shine and Myhre, 2020).

3. Results and discussion

We have evaluated the performance of the anharmonic QC workflow to predict REs by comparing our results with those reported by Pinnock et al. (Pinnock et al., 1995), Hodnebrog et al. (Hodnebrog et al., 2013) and Hodnebrog et al. (Hodnebrog et al., 2020). We used those different studies because of the increasing updates they have performed in both the IR cross sections (for which experimental data from different groups can show huge variations) and radiative forcing calculations.

3.1. The impact of band-shape function and half-width at half maximum

The impact of the employed band-shape function has been assessed at first by considering the following set of molecules: CFC-11, HCFC-22,

HCFC-141b, HCFC-142b, HFC-32, HFC-125, HFC-134a, HFC-143, HFC-152a whose structures are shown in Figure S1 of the supplementary material. For HFC-143 two conformers have been considered (see supplementary Figure S2), with that of lower symmetry presenting two equivalent rotamers. A series of tests using Gaussian and Lorentzian functions with different HWHMs in the range 10–40 cm^{-1} have been performed. Lorentzian broadening has systematically provided IREs more accurate than the Gaussian function, hence the former has been employed in our subsequent calculations, at variance with previous literature studies relying on the Gaussian curve (Bravo et al., 2010, 2011; Holtomo et al., 2022; Papanastasiou et al., 2018). Furthermore, the dependence of the IRE on the Lorentzian HWHM showed variations around 2%–3% when moving both from 10 to 20 cm^{-1} and from 20 to 30 cm^{-1}. While no significant statistical differences can be reported in the computed IREs when the HWHM ranges from 10 to 30 cm^{-1}, the general trend is that narrower HWHMs led to overestimation as shown in Fig. 2 where deviations between the presently computed IREs from reference values (Pinnock et al., 1995) are reported for the various levels of theory employed (the full list of IREs at the different HWHMs is given in Table S1 of the supplementary material). Across all the levels of theory, it is consistently observed that the mean IRE error for a HWHM of 30 cm^{-1} is lower than those obtained for HWHM of 10 and 20 cm^{-1}. Furthermore, except for the B3LYP functional, the median error between QC computed IREs and reference data (Pinnock et al., 1995) is within 7% for HWHM = 30 cm^{-1}, and also a narrower spread in the errors can be reported.

A few outliers can be spotted in Fig. 2: those obtained at the B2PLYP and rev-DSDPBEP86 levels of theory stem from the HFC-32 molecule, for which the IRE is underestimated by 17%–11%. These errors are not ascribable to a failure of the approach, but rather to the inaccurate cross section spectrum used in the first evaluation of the IRE taken as reference (Pinnock et al., 1995). Indeed, when updated REs are considered

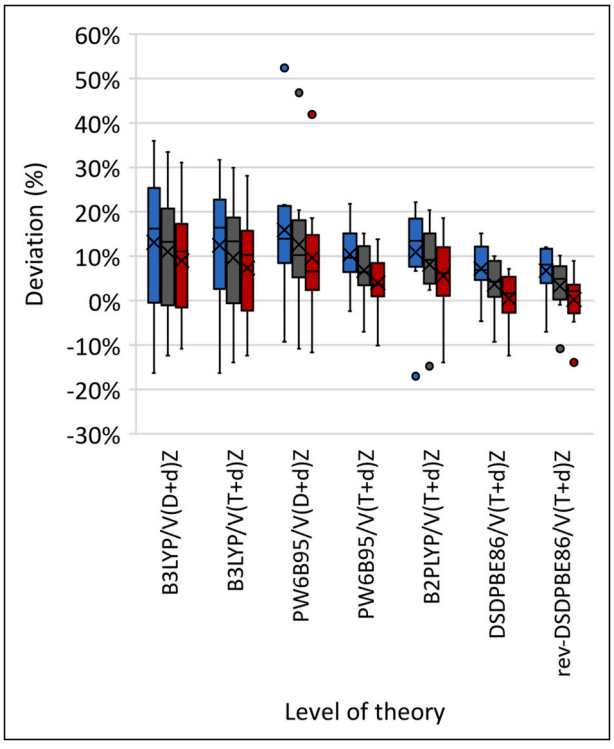

Fig. 2. Deviations of QC IREs from reference values (Pinnock et al., 1995) at different levels of theory and their dependence on the HWHM (10 cm^{-1}: blue; 20 cm^{-1}: grey; 30 cm^{-1}: red) of the Lorentzian broadening function. The black line and cross within each box represent the median and the mean, respectively, while circles mark outliers for the 95% confidence interval.

(Hodnebrog et al., 2013), an agreement better than 10% is recovered (vide infra) at all the levels of theory employed and for each HWHM. Conversely, the errors as large as 40% obtained for HFC-152 at the PW6B95/jul-cc-pV(D+*d*)Z level are due to an inadequacy of the basis set employed. Indeed, when the larger jul-cc-pV(T+*d*)Z basis is used, the computed IRE reconciles with the experimental counterparts with the expected accuracy. These results shed some light on the effect of the broadening function in the quantum chemically predicted REs that, to the best of our knowledge, has been previously considered only by Papanastasiou et al. (Papanastasiou et al., 2018). Even though the variation of the obtained REs with the HWHM amounts to a few percent, and it is certainly negligible in comparison to the level of theory employed, it can affect the accuracy of RE estimations. The impact of the HWHM is the more significant the narrower are the integration bins employed for the RE evaluation. While a HWHM of 30 cm^{-1} provides, on average, the most accurate REs, there can be exceptions, especially for heavy molecules (e.g. Br-containing) and when the IR features are at the edges of the 8–12 μm atmospheric window (as also pointed out for CF_4 in (Hodnebrog et al., 2013)). This is the case, for example, of Halon 1002 (CH_2Br_2) that exhibits a sharp absorption feature at about 1193 cm^{-1} close to the high-frequency edge of the atmospheric window, as shown in Fig. 3 where the cross section spectrum simulated theoretically in this work is compared to the experimental trace (National Institute of Standards and Technology (NIST)) and superimposed to the RF per unit cross section of the GAM (Pinnock et al., 1995). Conversely, the band located at about 653 cm^{-1} exactly matches the spectral range of the CO_2 bending mode. In such cases, even slight variations in the adopted HWHM can significantly affect the retrieved RE causing the wings of the band to fall out of the spectral windows or extend beyond (e.g.) the CO_2 feature. The latter effect was found relevant in the case of CH_2Br_2 resulting in an overestimation of the RE when using a HWHM of 30 cm^{-1}. This is not surprising given the sharp bands that characterize the longwave spectrum of this species coupled to the phenomenological description of the band-shape based on the use of an analytic function. When a more case-specific HWHM of 5 cm^{-1} is employed, the simulated band-shape reconciles with the observed one resulting in an IRE of 0.018 W m^{-2} $ppbv^{-1}$ in very good agreement with that derived based on experimental IR data (Hodnebrog et al., 2013).

3.2. Beyond the double-harmonic approximation

As previously stated, up to now QC calculations aimed at predicting REs have always been performed within the double harmonic approximation, eventually applying ad-hoc scaling factors to improve agreement with experimental fundamental transitions. While this approach partially corrects band positions, it has little impact on the overall harmonic spectrum pattern. Indeed, it cannot recover the so-called electrical anharmonicity (i.e. anharmonic contributions to IR intensities) and it fails to account for both combination bands and overtones as well as for vibrational energy and intensity redistributions caused by anharmonic resonances (Puzzarini et al., 2019; Tasinato et al., 2012). The effect of anharmonic contributions to vibrational transition frequencies can be appreciated by comparing harmonic and anharmonic simulations reported in Fig. 3 (blue and red traces, respectively) with the experimental spectrum. In passing, it should be noted that the double-peak nature of the absorption features appearing in the CH_2Br_2 experimental trace is not due to a doublet of transitions, but rather it is a characteristic band envelope. As it can be seen, harmonic calculations predict transition frequencies at 676 and 1228 cm^{-1}, thus overestimating experimental measurements by 20 and 30 cm^{-1}, respectively. Inclusion of anharmonicity yields a significantly more accurate placement of the bands, with peaks at 658 cm^{-1} and 1202 cm^{-1}, thus in close agreement with the experimental counterparts. In addition, it can be observed that even if small for this molecule, electrical anharmonicity modifies band intensities.

These effects are even more important when Fermi resonances

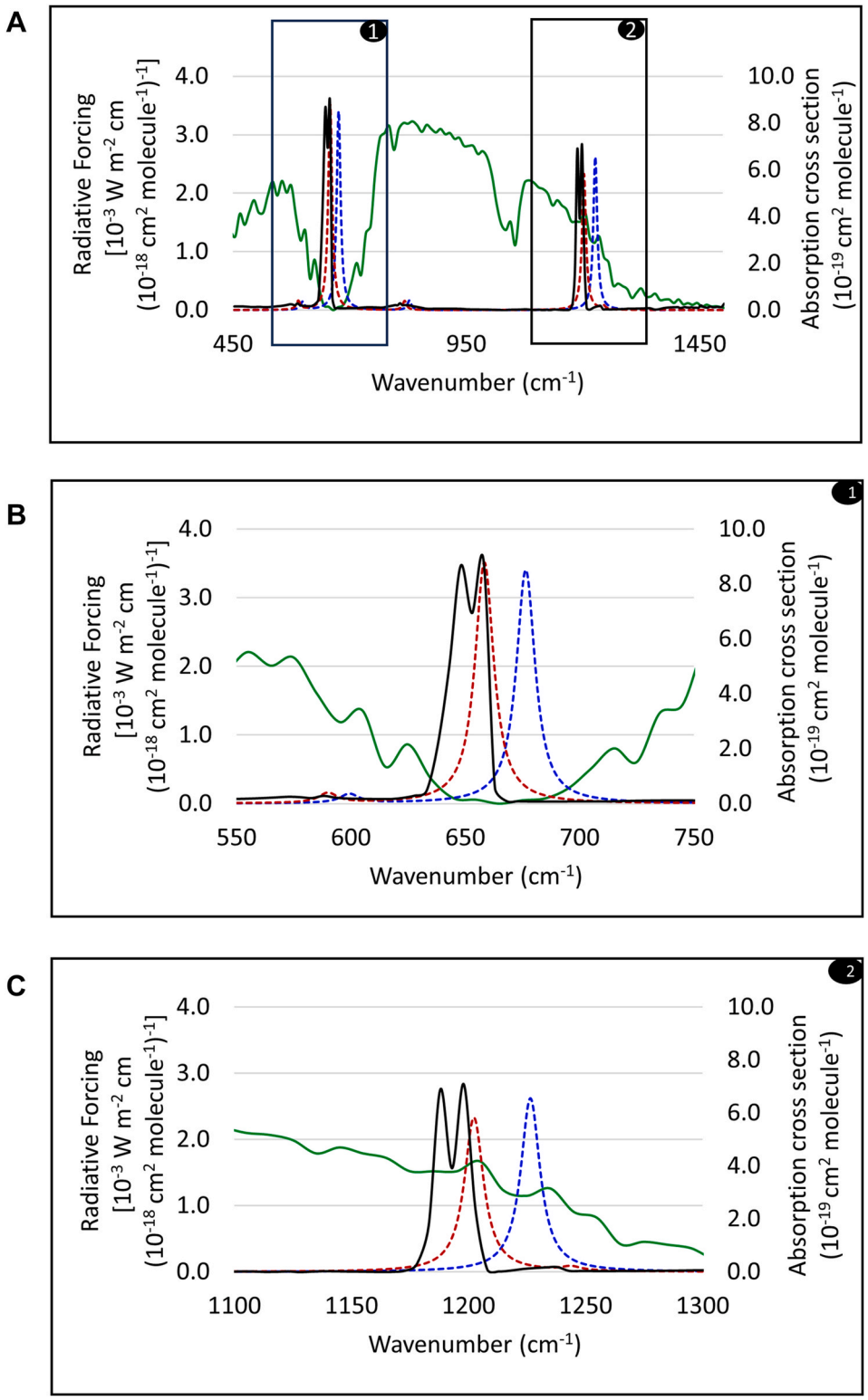

Fig. 3. IR absorption cross section spectrum of Halon 1002 (CH_2Br_2) simulated at DSDPBEP86/jun-cc-pVTZ level (blue dotted line: double-harmonic approximation; red dotted line: anharmonic effects included; stick spectrum convoluted with a Lorentzian function with a HWHM = 5 cm^{-1}) and comparison with the experimental absorbance spectrum (black continuous line). Spectra are superimposed to the Pinnock's curve for the RF per unit cross section of the GAM (green solid line). A magnified view of the regions 500–750 cm^{-1} and 1100–1300 cm^{-1} is reported in the middle and bottom panels, respectively.

between fundamentals and first overtones or binary combinations are present. In this respect, Fig. 4 compares the simulated harmonic (blue trace) and anharmonic (red trace) spectra of HFE-125 within the atmospheric window between 1000 and 1350 cm^{-1}. Even though the frequency shifts between anharmonic and harmonic spectra may appear quite systematic, they are difficult to properly reproduce using a scaling factor. More important is the significant weakening of the bands harmonically predicted at about 1300 cm^{-1} and 1180 cm^{-1} that move to about 1275 and 1150 cm^{-1}, respectively, in the anharmonic simulation. For the former band, the intensity weakening amounts to 12×10^{-19} cm

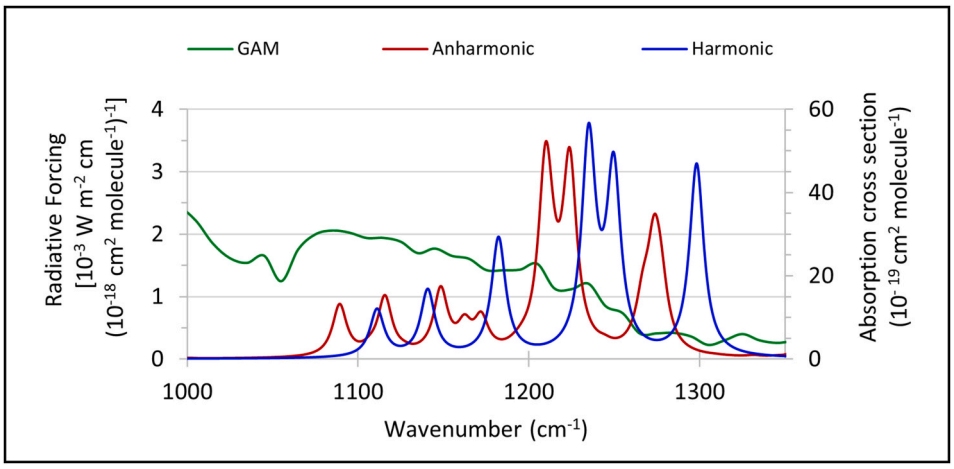

Fig. 4. IR absorption cross section spectrum of HFE-125 (CF_3OCHF_2) simulated at DSDPBEP86/jun-cc-pVTZ level (blue line: double-harmonic approximation, red line: anharmonic effects included. Spectra are superimposed to the RF per unit cross section of the GAM (green solid line) taken from Ref. (Hodnebrog et al., 2013).

molecule^{-1} whereas for the latter, the intensity reduction is about 17 × 10^{-19} cm molecule^{-1}. This is partly due a Fermi resonance with a nearby combination band located 1160 cm^{-1}, which indeed cannot be accounted for in the harmonic spectrum together with the signal at about 1170 cm^{-1} that arises as well from a combination vibration. Thus, it is evident that a simulation performed within the double harmonic approximation may neglect important spectral information, thus impacting on the retrieval of the RE as it will be discussed in the next subsection. While literature investigations have already pointed out that explicit inclusion of anharmonic contributions is essential for quantitative predictions of longwave vibrational spectra (Bloino et al., 2015; Carnimeo et al., 2013; Puzzarini et al., 2019; Tasinato et al., 2012), this aspect is still underrated in the studies devoted to the QC calculation of REs.

3.3. Quantum chemical prediction of radiative efficiencies

The previous sections have focused on tuning the QC workflow for the anharmonic evaluation of REs. In this section, the procedure is further validated by predicting EREs including stratospheric and lifetime adjustments and comparing them with the updated values provided in 2013 (Hodnebrog et al., 2013). The QC computed EREs obtained for 18 molecules including CFCs, HCFCs, HFCs, HFEs and halons (see Figure S1 of the supplementary information for molecular structures) are reported in Table 1 where they are compared with those listed by Hodnebrog et al. (2013), while a comprehensive list of results for each method can be found in the Supplementary Information (Table S2). As pointed out previously, EREs include both lifetime adjustment (see Eqn 4 and Eqn 5) and a 10% increase for the STA. In evaluating the overall absorption cross section spectrum, two conformers have been considered for CFC-113 (see supplementary Figure S2), of which the most stable one exists in two equivalent rotamers. As a test of consistency, the conformational search performed on HFE-125 has led to the identification of five conformers, which have reduced to the two expected ones after refinement at the DSDPBEP86-D3/jun-cc-pV(T+*d*)Z level of theory. The automatic characterization of the conformational landscape of HCFC-235ca2 has resulted in an ensemble of 22 structures, with 21 remaining after post-optimization. Among these, 5 lie within 1.3 kcal mol^{-1} (at 298 K) from the global minimum and hence the simulated absorption cross section spectrum stems from the Boltzmann average of six different conformers (which can be found in Figure S2). As it can be seen from Table 1, the QC computed EREs are in excellent agreement with those determined on the basis of experimental IR absorption cross section spectra. In particular, the DSDPBEP86/jun-cc-pV(T+d)Z level of theory reproduces the reference data with an average error of 5% and a maximum deviation of 13%, thus being on par with the accuracy expected from the use of experimental spectra. This finding is consistent with previous investigations that have highlighted the accuracy of double hybrid functionals, like (rev-) DSDPBEP86, in the prediction of vibrational spectroscopic properties (Barone et al., 2020; Bursch et al., 2022; Kozuch and Martin, 2013; Tasinato, 2014). The results yielded by the PW6B95 functional, with a mean absolute deviation (MAD) of 9%, are also remarkable, especially considering its lower computational cost. The correlation between QC computed EREs and reference data is illustrated in Fig. 5 for the B3LYP, PW6B95 and DSDPBEP86 functionals: the popular B3LYP provides the worst agreement (MAD = 22%, R^2 =

Table 1
QC anharmonic ERE (W m^{-2} ppbv^{-1}) obtained at different levels of theory and comparison with experimentally derived values.

Molecule	PW6B95/V (T+d)Z	DSDPBE86/V (T+d)Z	rev-DSDPBE86/V (T+d)Z	Ref. (Hodnebrog et al., 2013)
CFC-11	0.27	0.26	0.26	0.26
CFC-12	0.32	0.31	0.30	0.32
CFC-13	0.29	0.28	0.28	0.25
CFC-113	0.33	0.32	0.32	0.30
Halon 1002	0.01	0.01	0.01	0.01
Halon 1201	0.17	0.17	0.16	0.15
Halon 2301	0.15	0.15	0.15	0.14
Halon-1211	0.31	0.29	0.28	0.29
HCFC-22	0.21	0.20	0.20	0.21
HCFC-141b	0.16	0.16	0.16	0.16
HCFC-142b	0.20	0.20	0.20	0.19
HFC-32	0.11	0.11	0.11	0.11
HFC-125	0.25	0.24	0.24	0.23
HFC-134a	0.19	0.18	0.18	0.16
HFC-143	0.14	0.13	0.13	0.13
HFC-152a	0.11	0.10	0.11	0.10
HFE-125	0.47	0.44	0.44	0.41
HCFE-235ca2	0.48	0.45	0.46	0.41
MAD [a]	**9%**	**5%**	**6%**	
MD [b]	**9%**	**4%**	**4%**	
SD [c]	**7%**	**5%**	**6%**	

[a] Mean Absolute Deviation.
[b] Mean Deviation.
[c] Standard Deviation.

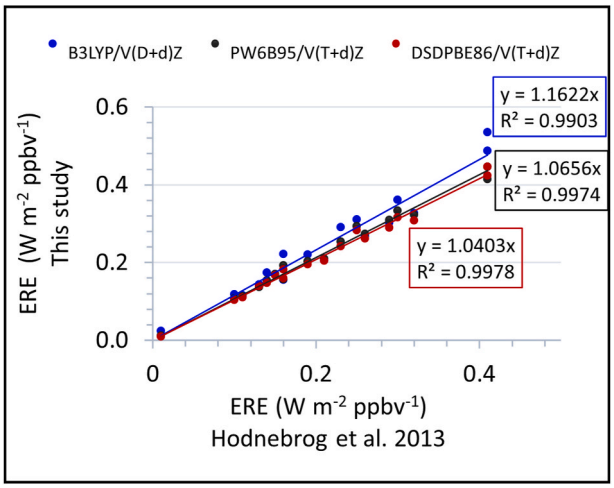

Fig. 5. Correlation between QC anharmonic effective radiative efficiencies obtained at different levels of theory and experimental reference values.

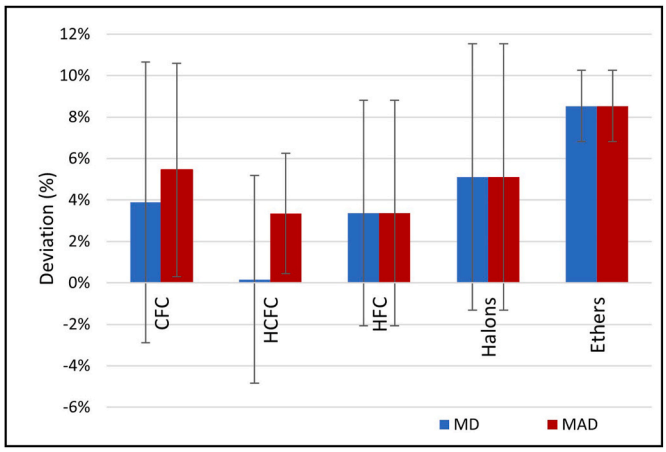

Fig. 6. Distribution among the categories of halocarbons considered in this work of percentage deviations between QC EREs obtained at DSDPBEP86/jun-cc-pV(T+*d*)Z level from the experimental counterparts (blue and red bars represent mean deviation and mean absolute deviation, respectively; black lines represent the standard deviation).

0.990), while an excellent correlation can be noted for both PW6B95 (MAD = 9%, R^2 = 0.996) and DSDPBEP86 (MAD = 5%, R^2 = 0.998) results. Even though, benchmark studies about the accuracy in the prediction of IR intensities are available in the literature (Barone et al., 2020; Boussessi et al., 2020; Carnimeo et al., 2013; Puzzarini et al., 2019; Tasinato, 2014; Yang et al., 2021), in order to better understand the causes of the significant discrepancies showed by the B3LYP functional irrespectively of the basis set employed, comparison has been made between the computed integrated absorption cross sections and the experimental counterparts as detailed in Table S3 of the SI where outcomes from the DSDPBEP86 DF are also reported. The results of this comparison mirror those drawn for REs with B3LYP reproducing measurements with an average error of 11% almost doubling that delivered by the DSDPBEP86 functional. Given the extended integration ranges used in the experimental determinations of integrated band intensities, that cover from hundreds to thousands of cm^{-1} and hence tends to smooth the effect of inaccurate transition frequencies, it can be concluded that imprecisions in both the calculated wavenumbers and intensities contribute to the observed deviations. In this respect, it has to be noted that, even though REs weights the IR absorption cross section spectrum by the GAM RF, their determination is very sensitive to both frequencies and intensities, because transitions should be (ideally) computed with an accuracy of at least 10 cm^{-1} in order to fit the right interval of the NBM (see equation (1)) and with the proper intensity. This also explains why the relative error in the REs for the B3LYP functional is larger by than that observed for the integrated intensities (wider integration intervals), while it remains almost the same for the DSDPBEP86 functional (more accurate for both frequencies and intensities).

The distribution of the deviations obtained at the DSDPBEP86 level among the various categories of halocarbons considered in this work is reported in Fig. 6. All of them present mean absolute deviations (MADs) within 9%. In particular, the quantum chemically predicted REs show remarkable accuracy for HCFCs, the MAD being less than 2%.

As previously pointed out, harmonic approximation neglects anharmonic effects and may introduce errors such as frequencies shifted compared to experiments, which can eventually be solved using a scaling factor. Errors in intensities, on the other hand, are not addressed, which can lead to a significant error in the predicted REs. In the case of HFE-125 there are appreciable differences between the harmonic and anharmonic absorption cross section spectra (see Fig. 4) which have been discussed in the previous subsection. For this molecule Blowers et al. (2008b) computed within the double-harmonic approximation an IRE of 0.49 W m^{-2} $ppbv^{-1}$ which is 24% higher than the 0.39 W m^{-2} $ppbv^{-1}$ obtained by Hodnebrog et al. using experimental spectra (Hodnebrog et al., 2013). Conversely, inclusion of anharmonic effects, as in our calculations, has yielded an IRE of 0.40 W m^{-2} ppv^{-1}, within 3% from the experimental value. Clearly, the RE retains high accuracy even after inclusion of lifetime correction and STA (see Table 1).

3.4. *Quantum chemical prediction of radiative efficiencies: case studies*

Finally, we have applied the anharmonic QC workflow to calculate the RE of selected molecules for which either literature data is contradictory (CFC-115, HFE-143a) or very limited (HFO-1123, R1122, HCFC-132b). For these species (molecular structures are reported in Figure S1), as well as for CFC-12, REs (collected in Table 2) have been evaluated by adopting the GAM worked out by Shine and Myhre (2020), which incorporates STA, thus demonstrating the robustness of our computational methodology to different atmospheric RF profiles. For CFC-12, a good agreement (−6%) with the recommended ERE value of 0.320 W m^{-2} $ppbv^{-1}$ (Hodnebrog et al., 2020) can be noted, thus being of the same quality as compared to the ERE obtained by using the GAM proposed by Hodnebrog et al., in 2013 (Hodnebrog et al., 2013). In the case of CFC-115, a striking deviation of 57% between the presently computed ERE and that appearing in the 2013 listing (0.202 W m^{-2} $ppbv^{-1}$) (Hodnebrog et al., 2013) has been observed. However, the deviation reduces to 24% when compared to the more recent update (0.263 W m^{-2} $ppbv^{-1}$) (Hodnebrog et al., 2020) which stems from the average of three different values spanning the range 0.205–0.321 W m^{-2} $ppbv^{-1}$. Interestingly, the computed ERE is in full agreement (3%

Table 2
QC anharmonic ERE (W m^{-2} $ppbv^{-1}$) obtained at DSDPBEP86/jun-cc-pV(T+d)Z level and comparison with available data.

Molecule	ERE		Lifetime (years)
	This work	Literature	
CFC-12	0.30	0.32 [a]	100 [a]
CFC-115	0.31	0.25 [a]	1020 [a]
HCFC-132b	0.18	0.19 [b]	3.5 [b]
HFE-143a	0.22	0.19 [a]	4.9 [a]
HFO-1123	0.0020	0.0018 [c]	3.8×10^{-3} [a]
R1122	0.02	0.02 [d]	5.5×10^{-2} [d]

[a] From Ref. (Hodnebrog et al., 2020).
[b] From Ref. (World Meteorological Organization (WMO), 2022).
[c] From Ref. (Tasinato et al., 2022).
[d] From Ref. (Pietropolli Charmet et al., 2022).

deviation) with the value of 0.321 W m^{-2} $ppbv^{-1}$ obtained by using the absorption cross section spectrum measured by Sharpe et al. (Sharpe et al., 2004). Hence, an ERE of 0.32 W m^{-2} $ppbv^{-1}$ appears the recommended value for CFC-115. In a similar way, the ERE here obtained for HFE-143a appears to overestimate by 25% the value listed in 2013 (0.177 Wm^{-2} $ppbv^{-1}$) (Hodnebrog et al., 2013). However, our result exhibits better agreement with the 2020 update (0.189 Wm^{-2} $ppbv^{-1}$) (Hodnebrog et al., 2020), with a deviation of 17%, and, remarkably, it matches even better with the most recent determination by the WMO (0.205 Wm^{-2} $ppbv^{-1}$) (World Meteorological Organization (WMO), 2022), the deviation reducing to only 8%.

The HFO-1123 molecule has been proposed as a refrigerant of the next generation, hence having an accurate RE is of primary importance because of its present-day industrial application. According to our calculations, the HFO-1123 IRE has resulted 0.105 W m^{-2} $ppbv^{-1}$ which is in good agreement (deviation of 5%) with the literature value that, according to the most recent investigation of its vibrational spectrum, amounts to 0.10 W m^{-2} $ppbv^{-1}$ (Tasinato et al., 2022). The ERE drops to about 2.0×10^{-3} W m^{-2} $ppbv^{-1}$ because of the huge contribution of the lifetime correction due to the very short atmospheric lifetime of this molecule.

R1122 ($ClHC{=}CF_2$) is a halogenated ethene currently employed in the production of some chemicals including fluoro-surfactants, textile finishing agents and organic silicon-fluorine modified resins. The only determination of its IRE has been carried out by Pietropolli Charmet et al. (Pietropolli Charmet et al., 2022) who obtained a value of 0.098 W m^{-2} $ppbv^{-1}$ in excellent agreement with the prediction here obtained at DSDPBEP86/jun-cc-pV(T+*d*)Z level (0.099 W m^{-2} $ppbv^{-1}$). Assuming a lifetime of 20 days (Pietropolli Charmet et al., 2022), an ERE of 0.02 W m^{-2} $ppbv^{-1}$ has been derived.

Lastly, the RE of HCFC-132b has not been subjected to any experimental determination and the only available data, collected in the WMO report (World Meteorological Organization (WMO), 2022), has been theoretically estimated using the double-harmonic approximation. Despite international regulations, this molecule has been recently detected in the atmosphere (Vollmer et al., 2021) with eastern China accounting for the major fraction of the global emissions (Yu et al., 2022). Indeed, while developed countries have almost phased out the production and consumption of HCFCs, developing countries are becoming the major contributors to their global emissions (Yi et al., 2021). Because of the recent atmospheric detection, and the lack of experimental investigations, the accurate determination of the HCFC-132b RE deserves particular attention. While the experimental analysis of the absorption cross section spectrum is currently being carried out in our group, and it will be the subject of a dedicated publication, the present anharmonic calculations have yielded an IRE of 0.19 W m^{-2} $ppbv^{-1}$ that lowers to an ERE of 0.18 W m^{-2} $ppbv^{-1}$ when STA and lifetime correction are applied. In passing, it should be noted that using the atmospheric lifetime theoretically determined on the basis of accurate kinetics calculations (1.9 years) (Rais et al., 2023) in place of the WMO recommended value of 3.5 years (World Meteorological Organization (WMO), 2022), marginally affects the resulting ERE, thus paving the way to a full *in silico* determination of REs.

To summarize, REs are employed in international reports on climate change and they are used by policymakers to drive mitigation actions contrasting global warming (Taddonio et al., 2023; Young et al., 2006). The compilation of REs, and hence of GWPs, rely on a careful selection of the determinations appeared in the literature, often on the basis of the accuracy estimated for the IR cross section spectrum, eventually followed by an average of different results. However, it is essential to acknowledge that different evaluations exist in the literature, as evident in cases such as CFC-115 and HFE-143a, which can impact the final estimate. In this framework, quantum chemical calculations can be employed either to trust experimental measurements or to predict REs in those cases where experiments are difficult to perform or for screening the global warming capacity of new replacement compounds.

4. Conclusions

The capacity of greenhouse gases emitted into the atmosphere to contribute to global warming is evaluated, as widely adopted in intergovernmental settlements on climate change, in terms of their REs. These depends, in addition to the atmospheric irradiance profile, on the IR absorption cross section spectrum of the target species. For the latter, experimental determinations, which can be performed with accuracies within 5% or even better, are of primary importance. However, in some instances reliable experimental measurements of the longwave absorption cross sections are extremely challenging or even impossible to be performed and quantum chemical predictions of the IR spectroscopic properties can be pursed as the viable solution. Evaluation of REs using quantum chemical calculations, however, up to now has been limited to the double-harmonic approximation, which presents several limitations and can significantly overestimate absorption cross sections thus introducing a bias in the computed REs.

This work has presented a computational workflow for the evaluation of REs, in which for the first time REs are accurately predicted using the IR absorption cross sections simulated theoretically with a full account of anharmonic effects without any adjustable parameter while featuring an automatic exploration of the conformational landscape. The procedure has been validated by considering a test of about twenty halocarbons, for which instantaneous and effective radiative efficiencies have been evaluated by using different GAMs and compared with available compilations based on experimental IR absorption cross sections. The effect of the broadening function, the only empirical parameter of the computational workflow, used to simulate the spectral band-shape on the retrieved REs have been explored, and the accuracy of different levels of theory has been assessed at first. Finally, the methodology has been applied to selected case studies, for which literature data are limited and to address some inconsistencies among REs experimentally determined. The results demonstrate that computational methods, involving both mechanical and electrical anharmonicity, can be effectively employed to consistently predict REs that match experimental data. In this respect, it should be noted that experimental cross section spectra inherently carry uncertainties, which can lead to errors of approximately 5% (Ballard et al., 2000; Hodnebrog et al., 2013; Pinnock et al., 1995). For heavier species, these uncertainties can increase to more than 10%. The consistency of our *in silico* predicted REs within this accuracy range strongly supports the reliability of our computational procedure. At this point, the validity of these conclusions with respect to temperature deserves a comment as the mean atmospheric temperature as well as that at higher altitudes are increasingly cooler than room temperature. Benchmark investigations have demonstrated that at room temperature the expected errors on the computed band intensities amount, on average, to c. a. 5% (Barone et al., 2020; Boussessi et al., 2020; Carnimeo et al., 2013; Puzzarini et al., 2019). However, it should be noted that QC IR transitions are computed, by definition, at zero temperature, hence the accuracy in the predictions can be expected to even improve moving toward lower temperatures. The current limitation of the approach is represented by the effective broadening function applied to simulate the overall band-shape. In fact, the band envelope observed experimentally, which can deviate from any bell-shaped curve and can cover wider spectral ranges, like in the case of *B*-type envelopes (especially for lighter molecules), is due to the molecular rotational motion that accompanies the vibrational transition. For the purpose, a further improvement will be devoted at reproducing the full ro-vibrational envelope by computing rotational spectroscopic parameters, as exemplified in the case of HFC-32 (Tasinato et al., 2012), to obtained a procedure free from any empirical parameter. Anyway, the results of the analysis here presented show only a moderate dependence on the selected HWHM which can be tuned within an extended range between 5 and 30 cm^{-1} with variations of a few percent in the obtained REs. As a general rule, high accuracies can be achieved with a broadening of 30 cm^{-1}, except in the case of molecules containing two or more

Br atoms, for which a HWHM of 5 cm^{-1} appears to be a more suitable choice. Furthermore, the accuracy of the predicted longwave spectra can be improved further, by adopting composite and hybrid methods (Ceselin et al., 2022; Pietropolli Charmet et al., 2022; Puzzarini et al., 2019; Tasinato et al., 2022). Work in these directions is ongoing in our group, with the final aim of providing an integrated workflow that, starting from the knowledge of the molecular structure, accurately estimates the radiative efficiency and the global warming potential. For the latter, atmospheric lifetimes, and hence rate constants, are fundamental quantities that should be predicted in addition to IR absorption cross sections. Overall, the outcomes of this work demonstrate that QC anharmonic IR cross section spectra can be used to estimate REs with an accuracy on par with that of experimental measurements, thus providing reliable data for screening purposes of new replacement compounds, as well as for feeding decision-making processes related to greenhouse gases and climate change.

CRediT authorship contribution statement

Daniela Alvarado-Jiménez: Investigation, Formal analysis, Data curation. **Nicola Tasinato:** Writing – review & editing, Validation, Supervision, Resources, Project administration, Funding acquisition, Conceptualization.

Declaration of competing interest

The authors declare that they have no known competing financial interests or personal relationships that could have appeared to influence the work reported in this paper.

Data availability

Data will be made available on request.

Acknowledgments

Prof. K.P. Shine is acknowledged for useful discussions. The STARK group is acknowledged for high-performance computing facilities. Scuola Normale Superiore is acknowledge for financial support through the project “Computational Modeling for Environmental Chemistry and Sustainability: from atmospheric monitoring to photo-catalysis”. This publication was produced while attending the PhD programme in PhD in Sustainable Development And Climate Change at the University School for Advanced Studies IUSS Pavia, Cycle XXXVIII, with the support of a scholarship co-financed by the Ministerial Decree no. 352 of April 9, 2022, based on the NRRP - funded by the European Union – Next Generation EU - Mission 4 ″Education and Research", Component 2 ″From Research to Business", Investment 3.3.

Appendix A. Supplementary data

Supplementary data to this article can be found online at https://doi.org/10.1016/j.atmosenv.2024.120839.

References

Alecu, I.M., Zheng, J., Zhao, Y., Truhlar, D.G., 2010. Computational thermochemistry: scale factor databases and scale factors for vibrational frequencies obtained from electronic model chemistries. J. Chem. Theor. Comput. 6, 2872–2887. https://doi.org/10.1021/ct100326h.

Andrews, T., Smith, C.J., Myhre, G., Forster, P.M., Chadwick, R., Ackerley, D., 2021. Effective radiative forcing in a GCM with fixed surface temperatures. J. Geophys. Res. Atmos. 126, e2020JD033880. https://doi.org/10.1029/2020JD033880.

Anthropogenic and natural radiative forcing. In: Climate Change 2013 – the Physical Science Basis: Working Group I Contribution to the Fifth Assessment Report of the Intergovernmental Panel on Climate Change; Intergovernmental Panel on Climate Change (IPCC), 2014. Cambridge University Press, Cambridge, pp. 659–740. https://doi.org/10.1017/CBO9781107415324.018.

Ballard, J., Knight, R.J., Newnham, D.A., Auwera, J.V., Herman, M., Lonardo, G.D., Masciarelli, G., Nicolaisen, F.M., Beukes, J.A., Christensen, L.K., Mcpheat, R., Duxbury, G., Freckleton, R., Shine, K.P., 2000. An intercomparison of laboratory measurements of absorption cross-sections and integrated absorption intensities for HCFC-22. J. Quant. Spectrosc. Radiat. Transfer 66, 109–128. https://doi.org/10.1016/S0022-4073(99)00211-3.

Barone, V., 2004. Anharmonic vibrational properties by a fully automated second-order perturbative approach. J. Chem. Phys. 122, 014108. https://doi.org/10.1063/1.1824881.

Barone, V., Ceselin, G., Fusè, M., Tasinato, N., 2020. Accuracy meets interpretability for computational spectroscopy by means of hybrid and double-hybrid functionals. Front. Chem. 8, 584203. https://doi.org/10.3389/fchem.2020.584203.

Barone, V., Ceselin, G., Lazzari, F., Tasinato, N., 2023. Toward spectroscopic accuracy for the structures of large molecules at DFT cost: refinement and extension of the nano-LEGO approach. J. Phys. Chem. A 127, 5183–5192. https://doi.org/10.1021/acs.jpca.3c01617.

Becke, A.D., 1993. Density-functional thermochemistry. III. The role of exact Exchange. J. Chem. Phys. 98, 5648–5652. https://doi.org/10.1063/1.464913.

Bloino, J., Biczysko, M., Barone, V., 2012. General perturbative approach for spectroscopy, thermodynamics, and kinetics: methodological background and benchmark studies. J. Chem. Theor. Comput. 8, 1015–1036. https://doi.org/10.1021/ct200814m.

Bloino, J., Biczysko, M., Barone, V., 2015. Anharmonic effects on vibrational spectra intensities: infrared, Raman, vibrational circular dichroism and Raman optical activity. J. Phys. Chem. A 119, 11862–11874. https://doi.org/10.1021/acs.jpca.5b10067.

Blowers, P., Hollingshead, K., 2009. Estimations of global warming potentials from computational chemistry calculations for CH_2F_2 and other fluorinated methyl species verified by comparison to experiment. J. Phys. Chem. A 113, 5942–5950. https://doi.org/10.1021/jp8114918.

Blowers, P., Moline, D.M., Tetrault, K.F., Wheeler, R.R., Tuchawena, S.L., 2008. Global warming potentials of hydrofluoroethers. Environ. Sci. Technol. 42, 1301–1307. https://doi.org/10.1021/es0706201.

Blowers, P., Tetrault, K.F., Trujillo-Morehead, Y., 2008. Global warming potential predictions for hydrofluoroethers with two carbon atoms. Theor. Chem. Acc. 119, 369–381. https://doi.org/10.1007/s00214-007-0394-3.

Boussessi, R., Ceselin, G., Tasinato, N., Barone, V., 2020. DFT meets the segmented polarization consistent basis sets: performances in the computation of molecular structures, rotational and vibrational spectroscopic properties. J. Mol. Struct. 1208, 127886. https://doi.org/10.1016/j.molstruc.2020.127886.

Bravo, I., Aranda, A., Hurley, M.D., Marston, G., Nutt, D.R., Shine, K.P., Smith, K., Wallington, T.J., 2010. Infrared absorption spectra, radiative efficiencies, and global warming potentials of perfluorocarbons: comparison between experiment and theory. J. Geophys. Res. 115, D24317. https://doi.org/10.1029/2010JD014771.

Bravo, I., Marston, G., Nutt, D.R., Shine, K.P., 2011. Radiative efficiencies and global warming potentials using theoretically determined absorption cross-sections for several hydrofluoroethers (HFEs) and hydrofluoropolyethers (HFPEs). J. Quant. Spectrosc. Radiat. Transfer 112, 1967–1977. https://doi.org/10.1016/j.jqsrt.2011.05.001.

Burkholder, J.B., Marshall, P., Bera, P.P., Francisco, J.S., Lee, T.J., 2020. Climate metrics for C1–C4 hydrofluorocarbons (HFCs). J. Phys. Chem. A 124, 4793–4800. https://doi.org/10.1021/acs.jpca.0c02679.

Bursch, M., Mewes, J.-M., Hansen, A., Grimme, S., 2022. Best-practice DFT protocols for basic molecular computational chemistry. Angew. Chem. Int. Ed. 134, e202205735. https://doi.org/10.1002/ange.202205735.

Carnimeo, I., Puzzarini, C., Tasinato, N., Stoppa, P., Charmet, A.P., Biczysko, M., Cappelli, C., Barone, V., 2013. Anharmonic theoretical simulations of infrared spectra of halogenated organic compounds. J. Chem. Phys. 139, 074310. https://doi.org/10.1063/1.4817401.

Ceselin, G., Salta, Z., Bloino, J., Tasinato, N., Barone, V., 2022. Accurate quantum chemical spectroscopic characterization of glycolic acid: a route toward its astrophysical detection. J. Phys. Chem. A 126, 2373–2387. https://doi.org/10.1021/acs.jpca.2c01419.

Chen, A., Chen, D., Hu, X., Harth, C.M., Young, D., Mühle, J., Krummel, P.B., O'Doherty, S., Weiss, R.F., Prinn, R.G., Fang, X., 2023. Historical trend of ozone-depleting substances and hydrofluorocarbon concentrations during 2004–2020 derived from satellite observations and estimates for global emissions. Environ. Pollut. 316, 120570. https://doi.org/10.1016/j.envpol.2022.120570.

Coheur, P.F., Clerbaux, C., Colin, R., 2003. Spectroscopic measurements of halocarbons and hydrohalocarbons by satellite-borne remote sensors. J. Geophys. Res.: Atmosphere 108, 4130. https://doi.org/10.1029/2002JD002649.

Forster, P., Storelvmo, T., Armour, K., Collins, W., Dufresne, J.-L., Frame, D., Lunt, D.J., Mauritsen, T., Palmer, M.D., Watanabe, M., Wild, M., Zhang, H., 2021. The earth's energy budget, climate feedbacks, and climate sensitivity. In: Climate Change 2021: the Physical Science Basis. Contribution of Working Group I to the Sixth Assessment Report of the Intergovernmental Panel on Climate Change. The Earth. https://doi.org/10.1017/9781009157896.009.

Forster, P.M., Smith, C.J., Walsh, T., Lamb, W.F., Lamboll, R., Hauser, M., Ribes, A., Rosen, D., Gillett, N., Palmer, M.D., Rogelj, J., von Schuckmann, K., Seneviratne, S.I., Trewin, B., Zhang, X., Allen, M., Andrew, R., Birt, A., Borger, A., Boyer, T., Broersma, J.A., Cheng, L., Dentener, F., Friedlingstein, P., Gutiérrez, J.M., Gütschow, J., Hall, B., Ishii, M., Jenkins, S., Lan, X., Lee, J.-Y., Morice, C., Kadow, C., Kennedy, J., Killick, R., Minx, J.C., Naik, V., Peters, G.P., Pirani, A., Pongratz, J., Schleussner, C.-F., Szopa, S., Thorne, P., Rohde, R., Rojas Corradi, M., Schumacher, D., Vose, R., Zickfeld, K., Masson-Delmotte, V., Zhai, P., 2023. Indicators of global climate change 2022: annual update of large-scale indicators of

the state of the climate system and human influence. Earth Syst. Sci. Data 15, 2295–2327. https://doi.org/10.5194/essd-15-2295-2023.
Frisch, M.J., Trucks, G.W., Schlegel, H.B., Scuseria, G.E., Robb, M.A., Cheeseman, J.R., Scalmani, G., Barone, V., Petersson, G.A., Nakatsuji, H., et al., 2016. Gaussian 16, Revision C.01. Gaussian Inc., Wallingford, CT.
González, S., Jiménez, E., Albaladejo, J., 2016. Assessment of the atmospheric loss processes initiated by OH radicals and sunlight, and the radiative efficiency for a series of hydrofluoroolefins, $CF_3(CF_2)_{X=1,3,5}CHCH_2$. Chemosphere 151, 45–54. https://doi.org/10.1016/j.chemosphere.2016.02.025.
Grimme, S., 2006. Semiempirical hybrid density functional with perturbative second-order correlation. J. Chem. Phys. 124, 034108. https://doi.org/10.1063/1.2148954.
Grimme, S., 2019. Exploration of chemical compound, conformer, and reaction space with meta-dynamics simulations based on tight-binding quantum chemical calculations. J. Chem. Theor. Comput. 15, 2847–2862. https://doi.org/10.1021/acs.jctc.9b00143.
Grimme, S., Antony, J., Ehrlich, S., Krieg, H., 2010. A consistent and accurate ab initio parametrization of density functional dispersion correction (DFT-D) for the 94 elements H-Pu. J. Chem. Phys. 132, 154104. https://doi.org/10.1063/1.3382344.
Grimme, S., Bannwarth, C., Shushkov, P., 2017. Exploration of chemical compound, conformer, and reaction space with meta-dynamics simulations based on tight-binding quantum chemical calculations. J. Chem. Theor. Comput. 13, 1989–2009. https://doi.org/10.1021/acs.jctc.7b00118.
Hibbert, D.B., 1993. Genetic algorithms in chemistry. Chemometr. Intell. Lab. Syst. 19, 277–293. https://doi.org/10.1016/0169-7439(93)80028-G.
Hodnebrog, Ø., Etminan, M., Fuglestvedt, J.S., Marston, G., Myhre, G., Nielsen, C.J., Shine, K.P., Wallington, T.J., 2013. Global warming potentials and radiative efficiencies of halocarbons and related compounds: a comprehensive review: halocarbon review. Rev. Geophys. 51, 300–378. https://doi.org/10.1002/rog.20013.
Hodnebrog, Ø., Aamaas, B., Fuglestvedt, J.S., Marston, G., Myhre, G., Nielsen, C.J., Sandstad, M., Shine, K.P., Wallington, T.J., 2020. Updated global warming potentials and radiative efficiencies of halocarbons and other weak atmospheric absorbers. Rev. Geophys. 58, e2019RG000691. https://doi.org/10.1029/2019RG000691.
Holtomo, O., Harison, N.M., Nsangou, M., Motapon, O., 2022. Infrared absorption cross section and radiative forcing efficiency features of four hydrofluoropolyethers: performance of some DFT functionals. Comput. Theor. Chem. 1214, 113798. https://doi.org/10.1016/j.comptc.2022.113798.
Basissetexchange.org https://www.basissetexchange.org/. Last access on 28 August 2024.
Kim, K.-H., Shon, Z.-H., Nguyen, H.T., Jeon, E.-C., 2011. A review of major chlorofluorocarbons and their halocarbon alternatives in the air. Atmos. Environ. 45, 1369–1382. https://doi.org/10.1016/j.atmosenv.2010.12.029.
Kozuch, S., Martin, J.M.L., 2013. Halogen bonds: benchmarks and theoretical analysis. J. Chem. Theor. Comput. 9, 1918–1931. https://doi.org/10.1021/ct301064t.
Leardi, R.J., 2001. Genetic algorithms in chemometrics and chemistry: a review. J. Chemom. 15, 559–569. https://doi.org/10.1002/cem.651.
Li, W., Spada, L., Tasinato, N., Rampino, S., Evangelisti, L., Gualandi, A., Cozzi, P.G., Melandri, S., Barone, V., Puzzarini, C., 2018. Theory meets experiment for noncovalent complexes: the puzzling case of pnicogen interactions. Angew. Chem. Int. Ed. 57, 13853–13857. https://doi.org/10.1002/anie.201807751.
Midgley, P., 1997. HCFCs and HFCs: halocarbon replacements for CFCs. Atmos. Environ. 31, 1095–1096. https://doi.org/10.1016/S1352-2310(96)00293-2.
National Institute of Standards and Technology (NIST)). NIST Chemistry WebBook, SRD 69: Methane, dibromo. NIST Chemistry WebBook, SRD 69. https://webbook.nist.gov/cgi/inchi?ID=C74953&Type=IR-SPEC&Index=1 (accessed 2023-September-7).
Papajak, E., Zheng, J., Xu, X., Leverentz, H.R., Truhlar, D.G., 2011. Perspectives on basis sets beautiful: seasonal plantings of diffuse basis functions. J. Chem. Theor. Comput. 7, 3027–3034. https://doi.org/10.1021/ct200106a.
Papanastasiou, D.K., Beltrone, A., Marshall, P., Burkholder, J.B., 2018. Global warming potentials for the C1-C3 hydrochlorofluorocarbons (HCFCs) included in the Kigali amendment to the Montreal protocol. Atmos. Chem. Phys. Discuss. 18, 6317–6330. https://doi.org/10.5194/acp-18-6317-2018.
Papasavva, S., Tai, S., Esslinger, A., Illinger, K.H., Kenny, J.E., 1995. Ab initio calculations of vibrational frequencies and infrared intensities for global warming potential of CFC substitutes: CF_3CH_2F (HFC-134a). J. Phys. Chem. 99, 3438–3443. https://doi.org/10.1021/j100011a006.
Papoušek, D., Aliev, M., 1982. Molecular Vibrational/Rotational Spectra. Elsevier, Amsterdam.
Peterson, K.A., Figgen, D., Goll, E., Stoll, H., Dolg, M., 2003. Systematically convergent basis sets with relativistic pseudopotentials. II. Small-core pseudopotentials and correlation consistent basis sets for the post-d group 16–18 elements. J. Chem. Phys. 119, 11113–11123. https://doi.org/10.1063/1.1622924.
Peterson, K.A., Shepler, B.C., Figgen, D., Stoll, H., 2006. On the spectroscopic and thermochemical properties of ClO, BrO, IO, and their anions. J. Phys. Chem. A 110, 13877–13883. https://doi.org/10.1021/jp065887l.
Pietropolli Charmet, A., Ceselin, G., Stoppa, P., Tasinato, N., 2022. The spectroscopic characterization of halogenated pollutants through the interplay between theory and experiment: application to R1122. Molecules 27, 748. https://doi.org/10.3390/molecules27030748.
Pinnock, S., Hurley, M.D., Shine, K.P., Wallington, T.J., Smyth, T.J., 1995. Radiative forcing of climate by hydrochlorofluorocarbons and hydrofluorocarbons. J. Geophys. Res. 100, 23227. https://doi.org/10.1029/95JD02323.
Pracht, P., Bohle, F., Grimme, S., 2020. Automated exploration of the low-energy chemical space with fast quantum chemical methods. Phys. Chem. Chem. Phys. 22, 7169–7192. https://doi.org/10.1039/C9CP06869D.
Pritchard, B.P., Altarawy, D., Didier, B., Gibson, T.D., Windus, T.L., 2019. A new basis set Exchange: an open, up-to-date resource for the molecular sciences community. J. Chem. Inf. Model. 59, 4814–4820. https://doi:10.1021/acs.jcim.9b00725.
Puzzarini, C., Bloino, J., Tasinato, N., Barone, V., 2019. Accuracy and interpretability: the devil and the holy grail. New routes across old boundaries in computational spectroscopy. Chem. Rev. 119, 8131–8191. https://doi.org/10.1021/acs.chemrev.9b00007.
Rais, N., Salta, Z., Tasinato, N., 2023. Thermochemistry and kinetics of the OH- and Cl-initiated degradation pathways of the HCFC-132b atmospheric pollutant. ACS Earth Space Chem. 7, 892–900. https://doi.org/10.1021/acsearthspacechem.3c00025.
Ramaswamy, V., Collins, W., Haywood, J., Lean, J., Mahowald, N., Myhre, G., Naik, V., Shine, K.P., Soden, B., Stenchikov, G., Storelvmo, T., 2019. Radiative forcing of climate: the historical evolution of the radiative forcing concept, the forcing agents and their quantification, and applications. Meteorol. Monogr. 59, 14.1–14.101. https://doi.org/10.1175/AMSMONOGRAPHS-D-19-0001.1.
Reimann, S., Elkins, J.W., Fraser, P.J., Hall, B.D., Kurylo, M.J., Mahieu, E., Montzka, S.A., Prinn, R.G., Rigby, M., Simmonds, P.G., Weiss, R.F., 2018. Observing the atmospheric evolution of ozone-depleting substances. C. R. Geosci. 350, 384–392. https://doi.org/10.1016/j.crte.2018.08.008.
Santra, G., Sylvetsky, N., Martin, J.M.L., 2019. Minimally empirical double-hybrid functionals trained against the GMTKN55 database: revDSD-PBEP86-D4, revDOD-PBE-D4, and DOD-SCAN-D4. J. Phys. Chem. A 123, 5129–5143. https://doi.org/10.1021/acs.jpca.9b03157.
Sharma, A., Walavalkar, M.P., Saha, A., Kawade, M., Kumar, A., Naik, P.D., 2019. Rate coefficients of reactions of 1-chlorocyclopentene with tropospheric oxidants at 298 K. Atmos. Environ. 199, 274–283. https://doi.org/10.1016/j.atmosenv.2018.11.046.
Sharpe, S.W., Johnson, T.J., Sams, R.L., Chu, P.M., Rhoderick, G.C., Johnson, P.A., 2004. Gas-phase databases for quantitative infrared spectroscopy. Appl. Spectrosc. 58, 1452–1461. https://doi.org/10.1366/0003702042641281.
Sherwood, S.C., Bony, S., Boucher, O., Bretherton, C., Forster, P.M., Gregory, J.M., Stevens, B., 2015. Adjustments in the forcing-feedback framework for understanding climate change. Am. Meteorol. Soc. 96, 217–228. https://doi.org/10.1175/BAMS-D-13-00167.1.
Shine, K.P., Myhre, G., 2020. The spectral nature of stratospheric temperature adjustment and its application to halocarbon radiative forcing. Ad. Model. Earth Syst. 12, e2019MS001951. https://doi.org/10.1029/2019MS001951.
Taddonio, K.N., Dreyfus, G.B., Andersen, S.O., Ravishankara, A.R., 2023. Trifluoroiodomethane as a precursor to high global warming potential climate pollutants: could the transformation of climatically benign CF_3I into potent greenhouse gases significantly increase refrigerant-related greenhouse gas emissions? Environ. Sci. Technol. 57, 11731–11737. https://doi.org/10.1021/acs.est.3c01079.
Tasinato, N., 2014. What are the spectroscopic properties of HFC-32? Answers from DFT. Int. J. Quant. Chem. 114, 1472–1485. https://doi.org/10.1002/qua.24716.
Tasinato, N., Pietropolli Charmet, A., Stoppa, P., Giorgianni, S., Buffa, G., 2010. Spectroscopic measurements of SO_2 line parameters in the 9.2 μm atmospheric region and theoretical determination of self-broadening coefficients. J. Chem. Phys. 132, 044315. https://doi.org/10.1063/1.3299274.
Tasinato, N., Pietropolli Charmet, A., Stoppa, P., Giorgianni, S., 2010. Determination of the vinyl fluoride line intensities by TDL spectroscopy: the object oriented approach of visual line shape fitting program to line profile analysis. Mol. Phys. 108, 677–685. https://doi.org/10.1080/00268970903468305.
Tasinato, N., Regini, G., Stoppa, P., Pietropolli Charmet, A., Gambi, A., 2012. Anharmonic force field and vibrational dynamics of CH_2F_2 up to 5000 cm^{-1} studied by fourier transform infrared spectroscopy and state-of-the-art ab initio calculations. J. Chem. Phys. 136, 214302. https://doi.org/10.1063/1.4720502.
Tasinato, N., Puzzarini, C., Barone, V., 2017. Correct modeling of cisplatin: a paradigmatic case. Angew. Chem. Int. Ed. 56, 13838–13841. https://doi.org/10.1002/anie.201707683.
Tasinato, N., Pietropolli Charmet, A., Ceselin, G., Salta, Z., Stoppa, P., 2022. In vitro and in silico vibrational–rotational spectroscopic characterization of the next-generation refrigerant HFO-1123. J. Phys. Chem. A 126, 5328–5342. https://doi.org/10.1021/acs.jpca.2c04680.
The Intergovernmental Panel on Climate Change. Reports IPCC. https://www.ipcc.ch/reports/(accessed 2023-December-16).
United Nations Environment Programme. The Montreal Protocol on Substances that Deplete the Ozone Layer. https://ozone.unep.org/treaties/montreal-protocol (accessed 2023-June-9).
Vainio, M.J., Johnson, M.S., 2007. Generating conformer ensembles using a multiobjective genetic algorithm. J. Chem. Inf. Model. 47, 2462–2474. https://doi.org/10.1021/ci6005646.
van Hoomissen, D., Papadimitriou, V.C., Burkholder, J.B., 2023. Low frequency (< 500 cm^{-1}) contribution to greenhouse gas radiative efficiency. Mol. Phys. 122, e2273412. https://doi.org/10.1080/00268976.2023.2273412.
Vollmer, M.K., Mühle, J., Henne, S., Young, D., Rigby, M., Mitrevski, B., Park, S., Lunder, C.R., Rhee, T.S., Harth, C.M., Hill, M., Langenfelds, R.L., Guillevic, M., Schlauri, P.M., Hermansen, O., Arduini, J., Wang, R.H.J., Salameh, P.K., Maione, M., Krummel, P.B., Reimann, S., O'Doherty, S., Simmonds, P.G., Fraser, P.J., Prinn, R.G., Weiss, R.F., Steele, L.P., 2021. Unexpected nascent atmospheric emissions of three ozone-depleting hydrochlorofluorocarbons. Proc. Natl. Acad. Sci. U.S.A. 118 (5). https://doi.org/10.1073/pnas.2010914118.
Wallington, T.J., Hurley, M.D., Nielsen, O.J., 2009. The radiative efficiency of $HCF_2OCF_2OCF_2CF_2OCF_2H$ (H-galden 1040x). Atmos. Environ. 43, 4247–4249. https://doi.org/10.1016/j.atmosenv.2009.05.046.

Wallington, T.J., Sulbaek Andersen, M.P., Nielsen, O.J., 2015. Atmospheric chemistry of short-chain haloolefins: photochemical ozone creation potentials (POCPs), global warming potentials (GWPs), and ozone depletion potentials (ODPs). Chemosphere 129, 135–141. https://doi.org/10.1016/j.chemosphere.2014.06.092.

World Meteorological Organization (WMO). World Meteorological Organization. World Meteorological Organization. https://wmo.int/(accessed 2023-December-16).

World Meteorological Organization (WMO), 2014. Scientific Assessment of Ozone Depletion: 2014; 55. World Meteorological Organization, Geneva, Switzerland, p. 416. https://csl.noaa.gov/assessments/ozone/2014/.

World Meteorological Organization (WMO), 2022. Scientific Assessment of Ozone Depletion: 2022, GAW Report No. 278. WMO, Geneva, Switzerland.

Yang, Q., Mendolicchio, M., Barone, V., Bloino, J., 2021. Accuracy and reliability in the simulation of vibrational spectra: a comprehensive benchmark of energies and intensities issuing from generalized vibrational perturbation theory to second order (GVPT2). Front. Astron. Space Sci. 8, 665232. https://doi.org/10.3389/fspas.2021.665232.

Yi, L., Wu, J., An, M., Xu, W., Fang, X., Yao, B., Li, Y., Gao, D., Zhao, X., Hu, J., 2021. The atmospheric concentrations and emissions of major halocarbons in China during 2009–2019. Environ. Pollut. https://doi.org/10.1016/j.envpol.2021.117190.

Young, C.J., Hurley, M.D., Wallington, T.J., Mabury, S.A., 2006. Atmospheric lifetime and global warming potential of a perfluoropolyether. Environ. Sci. Technol. 40, 2242–2246. https://doi.org/10.1021/es052077z.

Yu, Y., Xu, H., Yao, B., Pu, J., Jiang, Y., Ma, Q., Fang, X., O'Doherty, S., Chen, L., He, J., 2022. Estimate of hydrochlorofluorocarbon emissions during 2011–2018 in the Yangtze River Delta, China. Environ. Pollut. https://doi.org/10.1016/j.envpol.2022.119517.

Zhao, Y., Truhlar, D.G., 2005. Design of density functionals that are broadly accurate for thermochemistry, thermochemical kinetics, and nonbonded interactions. J. Phys. Chem. A 109, 5656–5667. https://doi.org/10.1021/jp050536c.